Influence of Nanozirconia on the Thermal Stability of Poly(methyl methacrylate) Prepared by *In Situ* Bulk Polymerization

Xinlong Wang, Lianghu Wu, Jin Li

School of Chemical Engineering, Nanjing University of Science and Technology, Nanjing 210094, China

Received 12 August 2009; accepted 5 December 2009
DOI 10.1002/app.31970
Published online 2 March 2010 in Wiley InterScience (www.interscience.wiley.com).

ABSTRACT: Nanozirconia (nano-ZrO_2) was prepared by the sol–gel method and incorporated into poly(methyl methacrylate) (PMMA) by the *in situ* bulk polymerization of methyl methacrylate. The structure of the nano-ZrO_2 was confirmed by X-ray diffraction (XRD), transmission electron microscopy, and Fourier transform infrared (FTIR) spectroscopy. The structure of the nano-ZrO_2 nanocomposites were studied by differential scanning calorimetry, FTIR spectroscopy, XRD, and scanning electron microscopy, and the results show that there were interactions between the nanoparticles and the polymer. The influence of the nano-ZrO_2 on the thermal stability of PMMA was investigated by thermogravimetric analysis (TGA). The results indicate that nano-ZrO_2 enhanced the thermal stability of the PMMA/nano-ZrO_2 nanocomposites. The effects of the heating rate in dynamic measurements (5–30°C/min) on kinetic parameters such as apparent activation energy (E_a) in TGA both in nitrogen and air were investigated. The Kissinger method was used to determine E_a for the degradation of pure PMMA and the PMMA/nano-ZrO_2 nanocomposites. The kinetic results show that the values of E_a for the degradation of the nanocomposites were higher than that of pure PMMA in air. © 2010 Wiley Periodicals, Inc. J Appl Polym Sci 117: 163–170, 2010

Key words: activation energy; nanocomposites; stabilization; thermal properties

INTRODUCTION

The incorporation of inorganic nanoparticles into a polymer matrix can significantly affect the thermal, optical, electrical, magnetic, and flammability properties.[1,2] Depending on practical applications, nanoscale particles, regardless of whether they are engineered or natural ones, so far seem to fall into four groups: metal oxides, nanoclays, nanotubes, and quantum dots. The group currently with the largest number of commercial nanomaterials is the metal oxides, such as zinc or titanium oxides, which are used in ceramics, chemical polishing agents, scratch-resistant coatings, cosmetics, and sunscreens.[3] Nanozirconia (nano-ZrO_2), as a common refractory material, has wide applications in many technological areas, such as gate dielectrics, high-performance transformation-toughened structural engineering ceramics, oxygen sensors, buffer layers for superconductor growth, catalysts, fuel-cell electrolytes, and damage-resistant optical coatings.[4] Poly(methyl methacrylate) (PMMA) is an important thermoplastic material and is widely used in numerous industries, including buildings, moldings, and decorative panels.[5] Polymer composites have been found to be successful in many applications, for example, organic batteries, microelectronics, nonlinear optics, and sensors. Because polymer nanocomposites have been a staple of the modern polymer industry, their durability under various environmental conditions and their degradability after their service life are also essential parts of the research. Therefore, it is important from a fundamental and practical point of view to understand the effects of the incorporation of nanoparticles on the physical and chemical properties of the composites.[6]

In this article, PMMA/nano-ZrO_2 nanocomposites were prepared by the bulk radical polymerization of methyl methacrylate (MMA) in the presence of the nano-ZrO_2. The influence of zirconia (ZrO_2) on the thermal stability of the PMMA matrix in nitrogen and air was investigated with thermogravimetric analysis (TGA). The thermal degradation kinetics of the PMMA/nano-ZrO_2 nanocomposites were also studied.

Correspondence to: X. Wang (wxinlong@sohu.com).
Contract grant sponsor: National Natural Science Foundation of China; contract grant number: 20473038.
Contract grant sponsor: Natural Science Foundation of the Education Committee of Jiangsu Province; contract grant number: 04KJB150066.

EXPERIMENTAL

Materials

Zirconium(IV) oxychloride octahydrate ($ZrOCl_2 \cdot 8H_2O$) was purchased from Sinopharm Chemical Reagent Co., Ltd. (Shanghai, China) and was used as received. MMA, *N,N*-dimethylaniline, and benzoyl peroxide were purchased from Shanghai Lingfeng Chemical Reagent, Ltd. (Shanghai, China). MMA was redistilled before use.

Preparation of the nano-ZrO_2

The nanoparticles were obtained by the sol–gel method, in a manner similar to that described in the literature.[7] $ZrOCl_2 \cdot 8H_2O$ (32 g) was dissolved in 500 mL of distilled water, and 25% aqueous ammonia was diluted with water 10 times as a precipitator. Then, the $ZrOCl_2$ solution was dropped into a precipitator at a speed of 3 mL/min under continuous stirring by a magnetic stirrer until the mixture pH reached 10. After the completion of dropping, the sol was continuously stirred for 2.5 h and maintained for stationary aging for 5 h to obtain $Zr(OH)_4$ precipitates. The precipitates were washed with distilled water and filtered until there were no more chloride ions (as checked by an $AgNO_3$ solution), and ethanol was added to the hydrogel to obtain an alcogel. The resulting gel was then dried in an oven at a temperature of 110°C for 12 h. The obtained samples were calcinated at a temperature of 800°C for 4 h in a static air atmosphere.

Preparation of the PMMA/nano-ZrO_2 nanocomposites

PMMA (4 g) was added to 94 g of MMA, and then, this mixture was oscillated for 24 h until PMMA was completely dissolved to obtain the MMA dispersion. To a 250-mL beaker, an appropriate amount of the nano-ZrO_2, 0.1 g of *N,N*-dimethylaniline, and 100 g of MMA dispersion were added and stirred for 10 min. Then, 0.3 g of benzoyl peroxide was added and stirred for 5 min. The bubbles in the contents of the beaker were removed *in vacuo.* Then, the mixture in the beaker was poured into a $10 \times 10 \times 0.5$ cm^3 glass mold, and the mold was heated to 40°C. After 24 h of polymerization at 40°C, plates for testing were obtained. The pure PMMA was prepared under the same experimental conditions. Using an MMA dispersion instead of pure MMA for the preparation of the nanocomposites increased the viscosity of the dispersion and reduced the possibility of particle aggregation and phase separation.

Characterization

The crystalline structure of the nano-ZrO_2 and the interaction between nano-ZrO_2 and the PMMA matrix were analyzed by X-ray diffraction (XRD; D8 ADVANCE, Bruker, Ettlingen, Germany) with Cu Kα radiation. The morphology of the nano-ZrO_2 was characterized by a JEOL 2100 transmission electron microscopy (TEM) apparatus (Electronic Corp., Tokyo, Japan). The morphology of the nanocomposites was observed by a Philips XL-305 Field Emission Gun–scanning electron microscopy instrument (Philips, Amsterdam, Holland). The thermal stability of PMMA and the PMMA/nano-ZrO_2 nanocomposites was measured by a nonisothermal thermogravimetric method with a DTG-60/60H simultaneous differential thermal analysis–thermogravimetry apparatus (Shimadzu Corp., Kyoto, Japan) from room temperature to 600°C, and the measurements were taken at heating rates of 5, 10, 20, and 30°C/min in a nitrogen atmosphere or in air at a flow rate of 20 mL/min. Differential scanning calorimetry (DSC) was

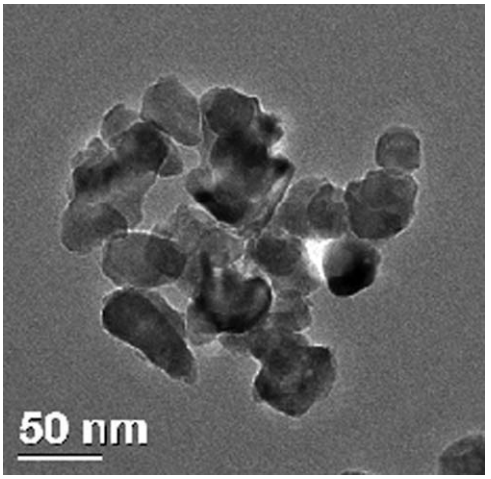

Figure 1 TEM photo of the nano-ZrO_2.

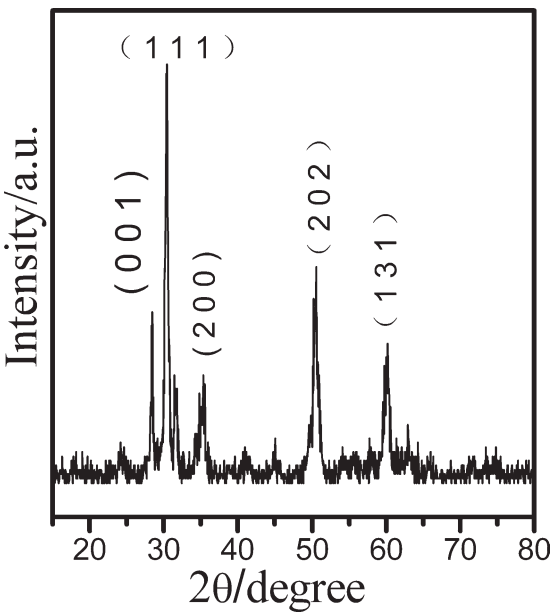

Figure 2 XRD pattern of the nano-ZrO_2.

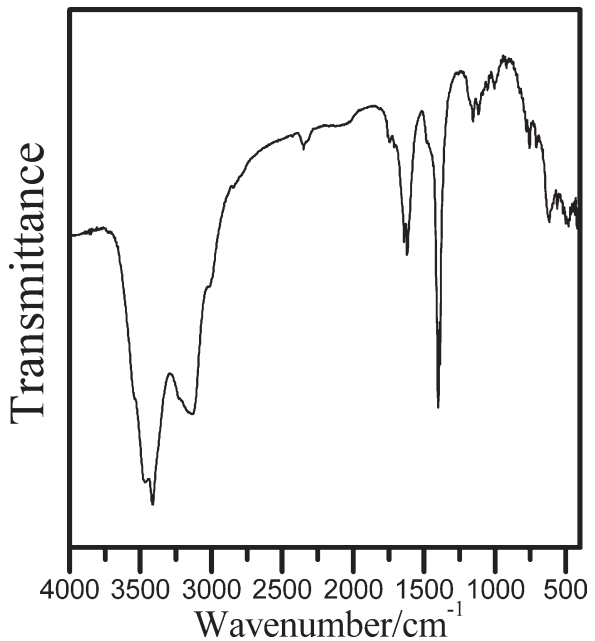

Figure 3 FTIR spectrum of the nano-ZrO_2.

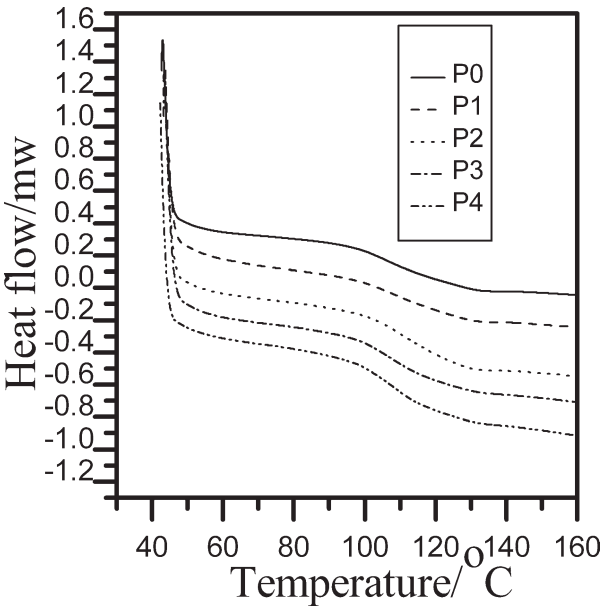

Figure 4 DSC curves of the nanocomposites.

done in a nitrogen atmosphere at a heating rate of 10°C/min with a Q80 DSC apparatus (TA Corp., New Castle, DE). Fourier transform infrared (FTIR) characterization was performed on an FTIR-8400S (Shimadzu Corp.) with KBr discs.

RESULTS AND DISCUSSION

Structure and characterization of the nano-ZrO_2

The shape and size distribution of the nano-ZrO_2 were observed by TEM. Figure 1 shows the image of the prepared nanoparticles. The diameter of the nano-ZrO_2 was less than 50 nm, and the sizes of particles were close to each other, which showed that the distribution was narrow. The typical XRD pattern of the prepared nano-ZrO_2 is shown in Figure 2. The diffraction peaks matching the 001, 111, 200, 202, and 131 crystal planes of the nano-ZrO_2 belonged to a tetragonal structure. The FTIR spectrum of the nano-ZrO_2 is shown in Figure 3. The bands at 3448 and 1621 cm^{-1} were attributed to stretching vibrations and bending vibrations of OH attached to the nano-ZrO_2. The band at 765 cm^{-1} was produced by Zr—O bending vibrations. Another bending band associated with Zr—O bonds and attributed to the presence of crystalline ZrO_2 was present at 619 cm^{-1}.[8]

Glass-transition temperature (T_g) of the nanocomposites

Pure PMMA and four samples of the PMMA/nano-ZrO_2 nanocomposites with different contents of nanoparticles were prepared by the *in situ* bulk polymerization of MMA under the same experimental conditions (Table I). The glass-transition behavior of the nanocomposites was investigated by DSC. The DSC curves of the five samples are shown in Figure 4. The values of T_g for all of the samples taken as the midpoint of the glass event are also listed in Table I. As shown in Table I, the values increased when the content of the nano-ZrO_2 increased, except in sample P5 because of the aggregation of the nano-ZrO_2 in the PMMA matrix. It is well known that there are many factors that affect the T_g of a polymer, such as the flexibility of the main chain, the type of substituents, and the configuration. The introduction of the nano-ZrO_2 may have restricted the mobility of the polymer chains, and accordingly, a significant shift in T_g of PMMA toward higher

TABLE I
Prepared PMMA and Nanocomposites

Sample	Content of nano-ZrO_2 (wt %)	T_g (°C)	$2\theta_1$ (°)	Residual solid (wt %)
P0	0	112.7	13.63	0
P1	0.5	116.6	13.38	90.5
P2	1.0	117.0	13.12	92.3
P3	3.0	117.2	12.97	94.6
P4	5.0	115.2	12.72	96.8

temperatures was observed. This is explained further in the following discussion.[9]

FTIR spectra of the PMMA/nano-ZrO_2 nanocomposites

The infrared spectra of pure PMMA and the nanocomposites are shown in Figure 5, and the expanded FTIR spectra ranging from 1800 to 1650 cm^{-1} are shown in Figure 6. The pure PMMA showed the carbonyl absorption at 1731.0 cm^{-1}. When nano-ZrO_2 was blended into PMMA, the carbonyl absorption began to shift to a lower wave number, but when the nano-ZrO_2 content reached 5%, it shifted to a higher wave number, which resulted from the aggregation of the nano-ZrO_2. This meant that there existed interaction between the nano-ZrO_2 and the PMMA matrix.[10,11]

XRD analysis of the PMMA/nano-ZrO_2 nanocomposites

The XRD patterns of the pure PMMA, nano-ZrO_2, and samples are shown in Figure 7. The amorphous diffraction peaks of PMMA were at about 13.6° ($2\theta_1$) and 29.1° ($2\theta_2$). Compared with sample P0, samples P1and P2 only had two amorphous diffraction peaks, and this meant that the nano-ZrO_2 had a good dispersability in the PMMA matrix and had no significant aggregation. The well-dispersed nano-ZrO_2 restricted the motion of the PMMA chain, and this led to a T_g increase. When the content of the nano-ZrO_2 reached 3%, two new peaks at 27.8 and 31.0° appeared and became dominant for P5, even the peaks at 29.7, 49.7, and 59.4° appeared. These

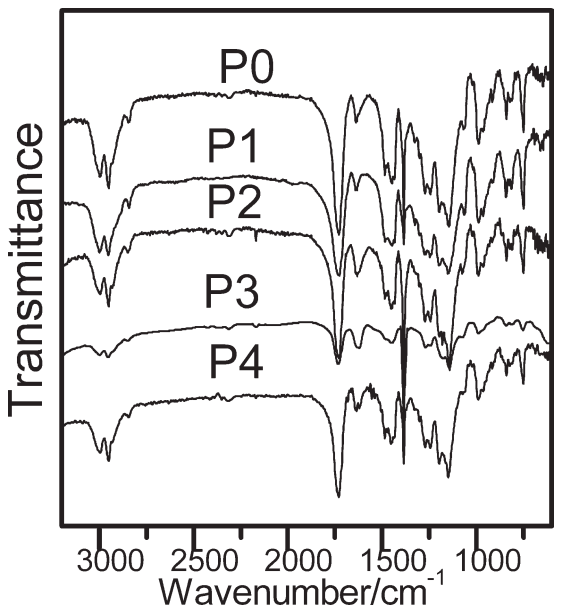

Figure 5 FTIR spectra of the pure PMMA and nanocomposites.

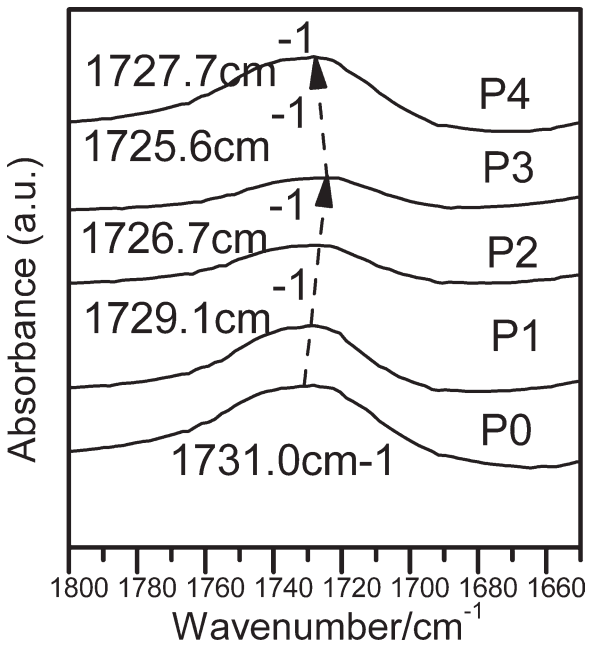

Figure 6 Expanded FTIR spectra of the pure PMMA and nanocomposites.

peaks just matched the peaks of the nano-ZrO_2, and this fully illustrated that, when the content of the nano-ZrO_2 was 3% or higher, the nanoparticles in the blends aggregated, which led to a T_g decrease. If the nano-ZrO_2 was indeed distributed throughout the PMMA matrix, $2\theta_1$ should have shifted to a smaller angle because of the nano-ZrO_2, which was expected to push the PMMA chain apart.[12] In fact,

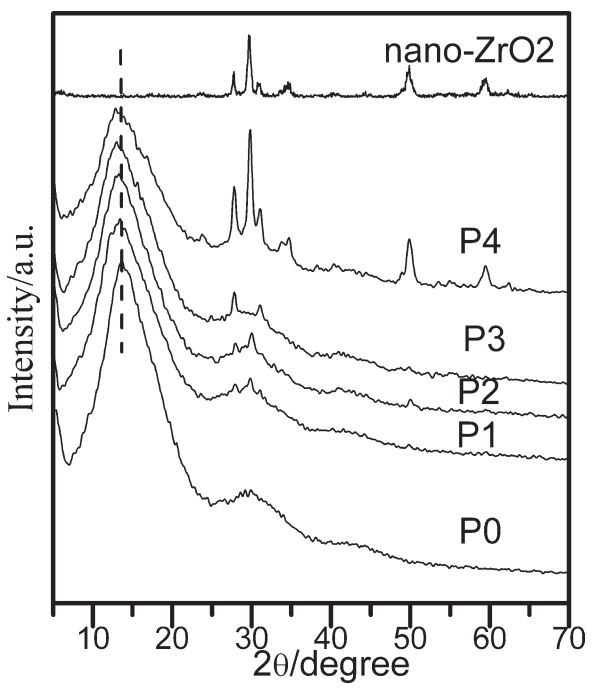

Figure 7 XRD patterns of the pure PMMA, nano-ZrO_2, and nanocomposites.

the $2\theta_1$ value shown in Table I had a slight shift to a smaller angle when the nano-ZrO_2 was added to the PMMA matrix, as shown in Figure 6. When 0.5% nano-ZrO_2 was added to PMMA, the $2\theta_1$ value decreased to 13.38°. When 1 and 3% nano-ZrO_2 were blended into the PMMA matrix, the $2\theta_1$ value decreased to 13.12 and 12.97°, respectively. Even when 5% nano-ZrO_2 was mixed into the PMMA matrix, the $2\theta_1$ value decreased to 12.72°. Furthermore, the amorphous diffraction peaks became wider as the content of the nano-ZrO_2 increased, as shown in Figure 6. All of these further indicated that there were interactions between the nanoparticles and the PMMA matrix.

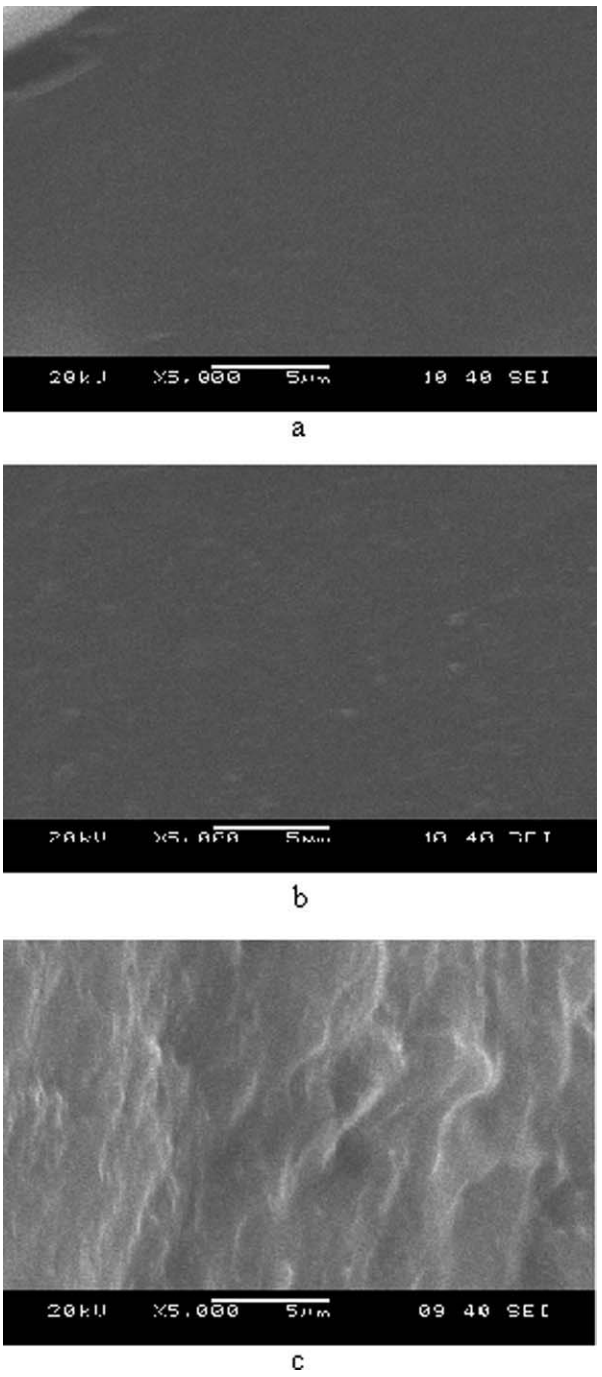

Figure 8 Scanning electron microscopy images of the pure PMMA and nanocomposites: (a) P0, (b) P2, and (c) P4.

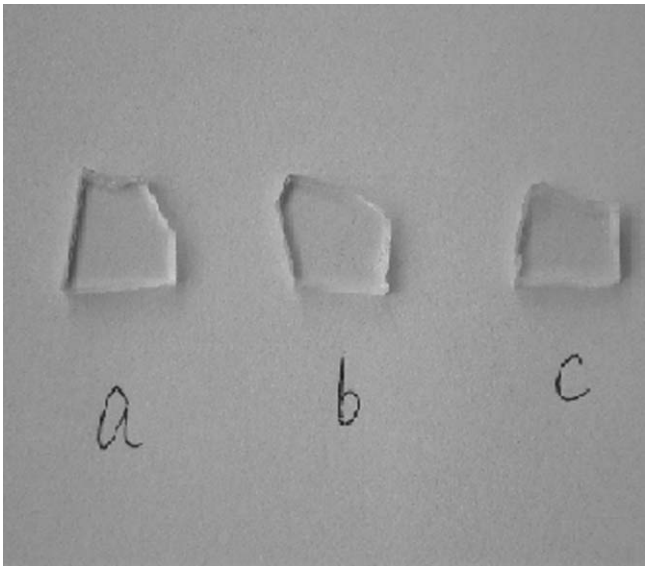

Figure 9 Photograph images of the pure PMMA and nanocomposites: (a) P0, (b) P2, and (c) P4.

Morphology of the PMMA/nano-ZrO_2 nanocomposites

The fracture surfaces of the samples are shown in Figure 8. As shown in the images, the nano-ZrO_2 was well dispersed in the PMMA matrix, and there

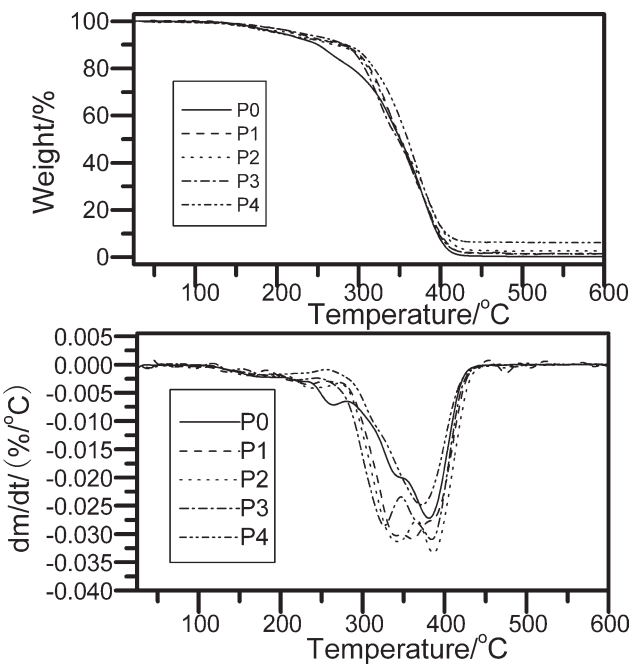

Figure 10 TGA and DTG curves of the PMMA and nanocomposites in nitrogen.

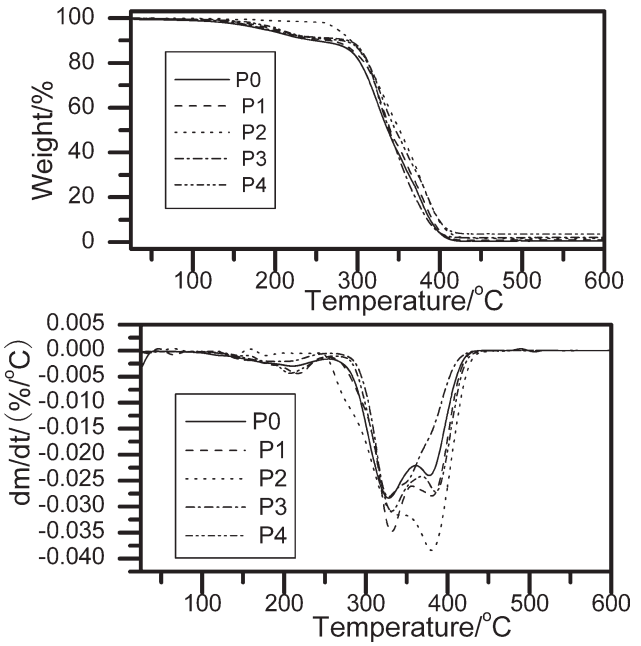

Figure 11 TGA and DTG curves of the PMMA and nanocomposites in air. dm/dt, derivative weight.

was no phase separation between the organic and inorganic components. When 1% nano-ZrO_2 was added to PMMA matrix, the inorganic particles were scattered inside the PMMA, and no obvious aggregation of the nano-ZrO_2 was indicated. When 5% nano-ZrO_2 was introduced, no clear particles were observed, and the emergence of bulges indicated strong interaction between the organic and inorganic phases without phase separation, which controlled the phase separation.

Solvent extraction results and photograph of PMMA and the nanocomposites

PMMA and the samples were extracted by tetrahydrofuran for a week, and the residual solid values are shown in Table I. As shown in Table I, the residual solid of PMMA was zero, but when 0.5% nano-ZrO_2 was introduced into the PMMA matrix, the value increased to 90.5%, and the residual solid value increased slightly as the content of nano-ZrO_2 increased. These results illustrate that there were interactions between the PMMA main chains and nano-ZrO_2 that prevented PMMA from dissolving in tetrahydrofuran.

Photographs of PMMA and the nanocomposites are shown in Figure 9. As shown in the images, the nanocomposites with 1.0% nano-ZrO_2 showed a high transparency similar to that of pure PMMA. When the amount of nano-ZrO_2 was 5%, the transparency decreased a little.

Thermal stability and thermal degradation kinetics of the PMMA/nano-ZrO_2 nanocomposites

The thermal stability of the PMMA/nano-ZrO_2 nanocomposites was tested by TGA. The TGA and differential thermogravimetry (DTG) curves of the samples under nitrogen and air are shown in Figures 10 and 11, respectively. As shown in Figures 10 and 11, the thermal degradation of pure PMMA and nearly all of the PMMA/nano-ZrO_2 nanocomposites under nitrogen and air showed three stages corresponding with the cleavage of head-to-head linkages, unsaturated vinyl ends, and random scission of the PMMA main chains.[13,14] The thermal decomposition temperatures (T_d's) of each step are listed in Table II. Under nitrogen, the T_d values of the three steps for pure PMMA were about 205.2, 285.2, and 354.7°C, but when nano-ZrO_2 was introduced, T_d for the first step increased slightly, and T_d for the third step increased obviously. However, T_d for the second step decreased. Under air, the T_d values for the first step and the second step increased obviously. However, T_d for the third step increased slightly or even decreased for P1. These proved that the incorporation of nano-ZrO_2 may have influenced some degradation processes of the nanocomposites, and the mechanisms were different in air and in nitrogen.

The TGA curves of the pure PMMA and the PMMA/nano-ZrO_2 nanocomposites performed

TABLE II
TGA Parameters of the Samples Under Nitrogen and Air

	T_d (°C)					
	Under nitrogen			Under air		
Identification	Step 1	Step 2	Step 3	Step 1	Step 2	Step 3
P0	205.2	285.2	354.7	177.8	253.9	360.4
P1	210.1	270.6	376.1	193.4	264.8	356.6
P2	215.1	272.5	366.4	204.3	272.0	362.0
P3	207.1	258.1	366.4	190.6	275.6	—
P4	210.0	261.0	—	188.6	279.5	370.3

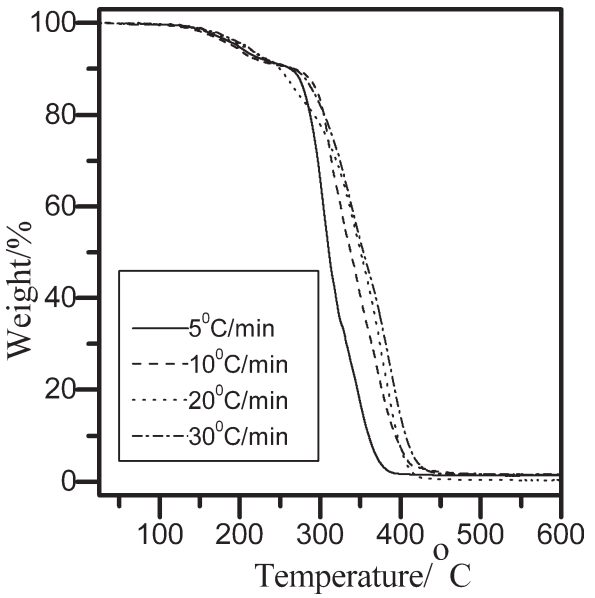

Figure 12 TGA curves of the pure PMMA at different heating rates under nitrogen.

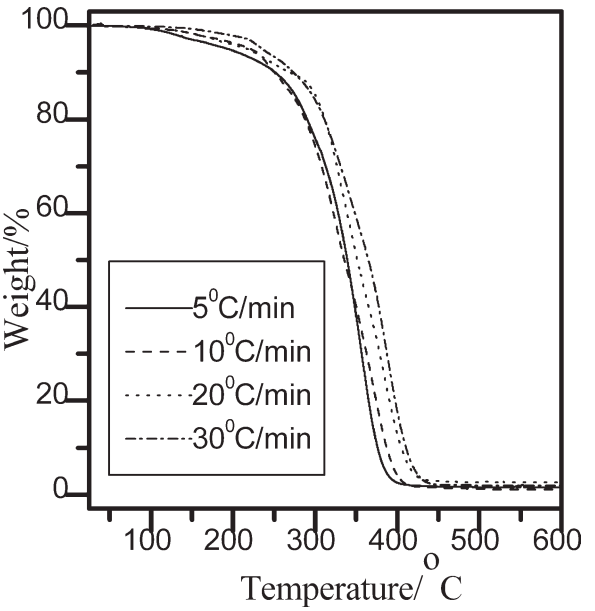

Figure 14 TGA curves of the nanocomposites at different heating rates under nitrogen.

under nitrogen and air at heating rates of 5, 10, 20, and 30°C/min are shown in Figures 12–15, respectively. To evaluate the degradation kinetics, the Kissinger method was used to analyze the TGA data. Kissinger put forward, for the period during the degradation of polymers, a simple but accurate relationship among apparent activation energy (E_a); the temperature of the maximum reaction rate at a constant heating rate (T_p), obtained from the DTG curves and listed in Table III; and the heating rate (β), as follows:[15]

$$\frac{d\ln\left(\frac{\beta}{T_p^2}\right)}{d\left(\frac{1}{T_p}\right)} = -\frac{E_a}{R} \tag{1}$$

where R is the gas constant.

Plots of $-\ln(\beta/T_p^2)$ against $1/T_p$ were created with the integral form of eq. (1), and E_a was calculated from the slope of the line. The values of E_a of every stage for pure PMMA and the nanocomposites are listed in Table III. Under nitrogen, the values of E_a for the first stage and the third stage of the

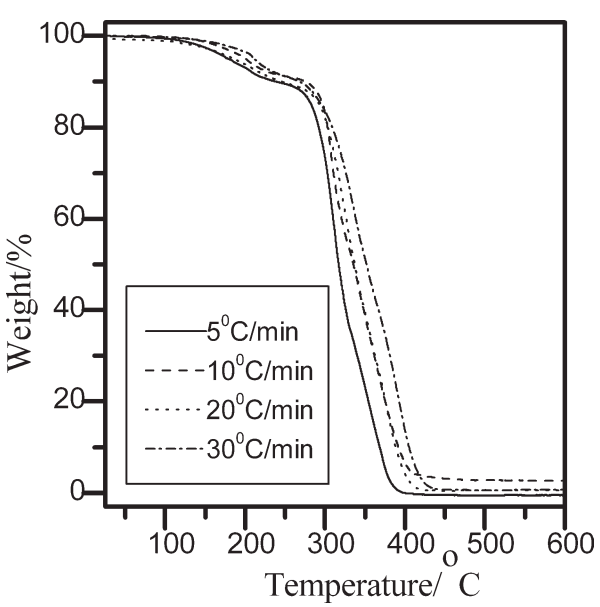

Figure 13 TGA curves of the pure PMMA at different heating rates under air.

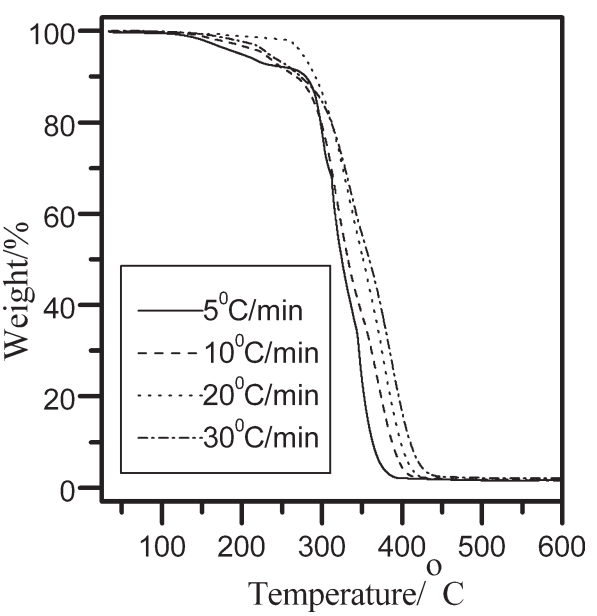

Figure 15 TGA curves of the nanocomposites at different heating rates under air.

TABLE III
E_a of Pure PMMA and the Nanocomposites Under Nitrogen and Air

Sample		Heating rate (°C/min)	T_p (°C)			E_a (kJ/mol)	Correlation coefficient
			Stage 1	Stage 2	Stage 3		
P0	Air	5	—	308.1	355.3	103.09 (stage 1)	1
		10	202.4	310.0	365.2	76.56 (stage 2)	0.9505
		20	214.5	326.3	377.6	120.42 (stage 3)	0.9951
		30	213.1	339.4	394.3		
	N_2	5	—	306.3	348.2	115.02 (stage 1)	1
		10	197.1	312.5	371.3	133.94 (stage 2)	0.9858
		20	218.7	343.1	377.4	138.28 (stage 3)	0.9958
		30	214.0	340.1	388.6		
P2	Air	5	—	301.5	346.2	121.38 (stage 1)	1
		10	219.1	319.3	371.4	99.40 (stage 2)	1
		20	230.2	338.5	379.3	131.08 (stage 3)	1
		30	229.1	338.3	389.6		
	N_2	5	—	309.1	358.2	122.90 (stage 1)	1
		10	222.3	329.2	373.5	130.25 (stage 2)	0.9939
		20	233.8	348.2	386.3	179.03 (stage 3)	0.9906
		30	230.0	345.2	391.4		

nanocomposites were larger than that of pure PMMA, but E_a for stage 2 was slightly lower than that of pure PMMA. Under air, when the nano-ZrO_2 was blended into PMMA, the three decomposition processes of the nanocomposites all showed larger values of E_a compared with pure PMMA. The increase in E_a could be explained by the action of the nano-ZrO_2 with the PMMA molecules, which inhibited the depolymerization of PMMA or reacted with the decomposition products of PMMA to interrupt and suppress the free-radical depolymerization. Also, under air, E_a of the second stage was lower than that of the first stage. This indicated that oxygen may have enhanced the degradation of PMMA at high temperatures but suppressed the degradation at lower temperatures. Also, as shown in Table III, the E_a values of the three stages in air were lower than those under nitrogen because of oxygen's participation.[16]

CONCLUSIONS

The PMMA/nano-ZrO_2 nanocomposite samples with different amounts of nano-ZrO_2 were synthesized by the bulk radical polymerization of MMA. The TGA results both in nitrogen and air show that the thermal T_d of each step was affected by the loading of the nano-ZrO_2. The TGA kinetics results by the Kissinger method show that E_a of the degradation of pure PMMA was lower than that of the nanocomposite; this indicated that nano-ZrO_2 had an effect on the degradation process of PMMA. The introduction of nano-ZrO_2 restricted the mobility of the polymer chains and enhanced the T_g of the nanocomposites.

References

1. Kickelbick, G. Prog Polym Sci 2003, 28, 83.
2. Caseri, W. Macromol Rapid Commun 2000, 21, 705.
3. Vaia, R. A.; Wagner, H. D. Mater Today 2004, 7, 32.
4. Kumari, L.; Du, G.-H.; Li, W.-Z.; Vennila, R. S.; Saxena, S. K.; Wang, D.-Z. Ceram Int 2009, 35, 2401.
5. Wang, G.-A.; Wang, C.-C.; Chen, C.-Y. Polym Degrad Stab 2006, 91, 2683.
6. Kuljanin-Jakovljevic, J.; Marinovic-Cincovic, M.; Stojanovic, Z.; Krkljes, A.; Abazovic, N. D.; Comor, M. I. Polym Degrad Stab 2009, 94, 891.
7. Caracoche, M. C.; Rivas, P. C.; Cervera, M. M.; Caruso, R.; Benavídez, E.; Oscar, D. S.; Escobar, M. E. J Am Ceram Soc 2000, 83, 377.
8. Lopez, T.; Tzompantzi, F.; Hernandez-Ventura, J.; Gomez, R. J Sol–Gel Sci Tech 2002, 24, 207.
9. Laachachia, A.; Cocheza, M.; Ferriola, M.; Lopez-Cuestab, J. M.; Leroy, E. Mater Lett 2005, 59, 36.
10. Janos, M.; Bela, P. J Ind Eng Chem 2008, 14, 535.
11. Feng, Y.; Jia, Y.; Xu, H.-Y. J Appl Polym Sci 2009, 111, 2684.
12. Kopesky, E. T.; Haddad, T. S.; McKinley, G. H.; Cohen, R. E. Polymer 2005, 46, 4743.
13. Lewis, E. M.; Dotsevi, Y. S.; Gordon, M. C. Macromolecules 1989, 2, 4652.
14. Hirata, T.; Kashiwagi, T.; Brown, J. E. Macromolecules 1985, 18, 1410.
15. Kissinger, H. E. Anal Chem 1957, 29, 1702.
16. Arisawa, H.; Brill, T. B. Combust Flame 1997, 109, 415.